Rare Metal Materials and Engineering
Volume 54, Issue 10, October 2025
Available online at www.rmme.ac.cn

Science Press

Cite this article as: Wang Youliang, Jiang Zhe, Zhang Wenjuan, et al. Ultra-precision Polishing of Outer Surface of Tube Using Magnetic Compound Fluid Wheel[J]. Rare Metal Materials and Engineering, 2025, 54(10): 2429-2439. DOI: https://doi.org/10.12442/j.issn.1002-185X.20240558.

ARTICLE

Ultra-precision Polishing of Outer Surface of Tube Using Magnetic Compound Fluid Wheel

Wang Youliang[1,2], Jiang Zhe[1], Zhang Wenjuan[3], Yin Xincheng[1,2], Liang Bo[1]

[1] School of Mechanical and Electrical Engineering, Lanzhou University of Technology, Lanzhou 730050, China; [2] Key Laboratory of Digital Manufacturing Technology and Application, Ministry of Education, Lanzhou University of Technology, Lanzhou 730050, China; [3] State Key Laboratory of Advanced Processing and Recycling of Nonferrous Metals, Lanzhou University of Technology, Lanzhou 730050, China

Abstract: A novel method employing magnetic compound fluid (MCF) wheel was proposed for polishing the outer surface of stainless steel tube. Firstly, a polishing apparatus was constructed. In addition, the distribution of the magnetic field of MCF wheel on the workpiece surface was explored by Maxwell software and Tesla meter, and the relationship between magnetic field distribution and material removal (MR) on the workpiece surface was investigated. Then, MR model was established and proved by the experiment results under specific experiment conditions. Finally, the influence laws of carbonyl iron powder particle size d_{CIP}, abrasive particle size d_{AP}, magnet speed n_m, workpiece speed n_c, and MCF supply amount V on surface roughness R_a and reduction rate were investigated through experiments, and the mechanisms of different parameters on surface quality were explored. Results show that the magnetic induction intensity during polishing is positively correlated with the polished profile of the workpiece. The trend of MR simulation is consistent with that of the experiment value, which proves the accuracy of MR model. When the revolution speeds of magnet and workpiece are 200 and 5000 r/min, respectively, and 2 mL MCF slurry containing 50wt% carbonyl iron powder (15 μm), 12wt% abrasive particle (7 μm), 3wt% α-cellulose, and 35wt% magnetic fluid was used, the final surface roughness decreases from 0.411 μm to 0.007 μm. After polishing for 100 min, the reduction rate is 98.297%, demonstrating that this method is appropriate for polishing the outer surface of tube.

Key words: magnetic compound fluid; stainless steel tube; polishing; surface roughness

1 Introduction

Stainless steel is widely used in aerospace, petroleum engineering, nuclear industry, biomedical, and other fields, because of its excellent corrosion resistance, high strength, and excellent plasticity and toughness[1–3]. In the medical field, stainless steel capillary stents have become an effective method to treat coronary artery disease[4–5]. Studies have shown that the rougher the outer surface of the stainless steel capillary tube, the greater the area of the stent exposed to the blood, and the greater the possibility of thrombus occurrence. Therefore, the stainless steel serving as a support material should have high surface quality. In order to ensure the surface quality of stainless steel capillary tubes, it is necessary to polish the outer surface of stainless steel tubes to ensure that they have good shape accuracy and surface finish. Due to the complex structure and small size of the scaffolds, traditional mechanical polishing cannot meet the surface quality requirements of stainless steel[6]. Traditional grinding can cause minor scratches and pits on the surface of stainless steel. In order to solve the abovementioned problems, a multi-energy field-assisted ultra-precision polishing process was proposed, which mainly includes chemical mechanical polishing[7], abrasive flow polishing[8], jet polishing[9], electrophoretic polishing[10], and magnetic field-assisted polishing[11].

Multi-energy field-assisted polishing and other polishing processes are mainly characterized by energy fields, such as chemical field, ultrasonic field, fluid field, and magnetic field[12], to assist material removal (MR), thereby obtaining

Received date: October 28, 2024
Foundation item: National Natural Science Foundation of China (52265056, 52262013); Lanzhou Young Talent Program (2023-QN-38); Natural Science Foundation of Gansu Province (23JRRA776)
Corresponding author: Wang Youliang, Ph. D., Associate Professor, Key Laboratory of Digital Manufacturing Technology and Application, Ministry of Education, Lanzhou University of Technology, Lanzhou 730050, P. R. China, E-mail: wangyouliang20@163.com

ultra-smooth surfaces. Magnetic field-assisted polishing has the advantages of low cost and high polishing precision, and it has been widely used in industrial manufacture. Magnetic field-assisted polishing technique can be divided into magnetic fluid (MF) polishing, magnetorheological fluid (MRF) polishing, and magnetic compound fluid (MCF) polishing. MF polishing involves the addition of abrasive particles into MF. In the processing process, the polishing liquid has good particle dispersion, but its viscosity is low, resulting in low polishing efficiency[13–16]. MRF polishing is based on MF with the addition of micro-sized iron powder particles, which solves the problem of low viscosity of the polishing fluid, but the dispersion of the particles is inferior[17–19]. MCF has the advantages of both MF and MRF, namely, good particle dispersion and fine viscosity[20–21].

MCF polishing technique has shown excellent polishing properties[22]. Guo et al[23] polished polymethyl methacrylate (PMMA) by MCF, and it was reported that without abrasive particles, the zirconia-coated carbonyl iron powder (CIP) MCF slurry exhibited larger polishing power and resulted in a smoother surface, compared with the conventional MCF slurry. Guo et al[24] also used MCF to spot-polish the optical glass, revealing that shear had a more significant effect on the material removal ratio (MRR) than pressure, and a related MRR model was proposed. Wang et al[25] employed MCF for high-precision polishing of miniature V-grooves, and the results indicated that MCF could significantly improve surface quality while maintaining the high shape accuracy of the miniature V-grooves. Wang et al[26] also used MCF to polish electroless Ni-P-plated STAVAX steel, and the surface roughness was reduced to 4 nm by investigating the relationship of the particle sizes of CIPs and abrasive particles with the working gap[26]. In addition, Wang et al[27] further used MCF to polish GaAs wafers, and the surface roughness was reduced to 0.82 nm after polishing by water-based MCF containing abrasive particles with diameter of 0.3 μm at MR rate of 13.5 μm/h. Fan et al[28] proposed an optimization method for MCF polishing and achieved a balance between high-quality surface polishing and high dimensional accuracy through experiment modeling combined with a multi-objective particle swarm optimization algorithm. Jiao et al[29] applied MCF to polish optical glass and investigated the effect of magnetic field distribution on MR efficiency of MCF wheel polishing, showing that higher MRRs could be achieved using MCF wheels with NS-SN magnetic pole distribution. A doughnut-shaped MCF tool was used to polish spherical surfaces, and the effect of MCF composition on the polishing results was explored[30]. It was found that the concentration of CIP and the size of abrasive particles had a significant effect on MRR and surface quality[30].

Currently, MCF has been widely applied to ultra-precision polishing of various materials, such as glass, oxygen-free copper, PMMA, nickel-plated STAVAX steel, and GaAs. In this study, a polishing device for the outer surface of stainless steel tube was designed based on MCF polishing wheel. The MR model was established, and the feasibility of this model was verified. The influence of different machining parameters on the surface roughness of the workpiece using MCF was investigated, and the optimal experimental parameters of the MCF polishing wheel were determined to realize ultra-precision machining of the outer surface of stainless steel tube.

2 Polishing Principle

Fig. 1 shows the polishing principle of the outer surface of the tube using MCF polishing wheel. MCF polishing wheel is composed of a ring magnet with uniformly distributed MCF, which is fixed on the main shaft driven by a servo motor and rotates at a fixed speed n_m. The stainless steel tube is placed with a direct processing gap δ below the ring magnet. The stainless steel tube is driven by the electric spindle at a fixed speed n_c. MCF polishing slurry is composed of micron-sized CIP, α-cellulose, micron-sized non-magnetic abrasive particles, and water-based MF containing nanometer-sized Fe_3O_4. Under the action of external magnetic field, MCF slurry becomes a Bingham medium with a certain viscosity, forming flexible polishing tool in the polishing area. CIPs within MCF slurry form a chain structure along the magnetic field line, and the length of the chain structure is related to the strength of the applied magnetic field. The α-cellulose was inserted between multiple chain structures to improve the viscosity of MCF. The abrasive particles tend to move to the workpiece surface under the action of magnetic force. When the polishing wheel rotates, it drives MCF to rotate together. The wedge effect at the entrance of the polishing area causes MCF to compress, creating significant magnetizing pressure and shear force. This phenomenon results in mutual motion between the Al_2O_3 particles on the surfaces of MCF and tube, thereby achieving micro-removal of materials from the tube.

3 Experiment

The appearance of the device of MCF polishing wheel is

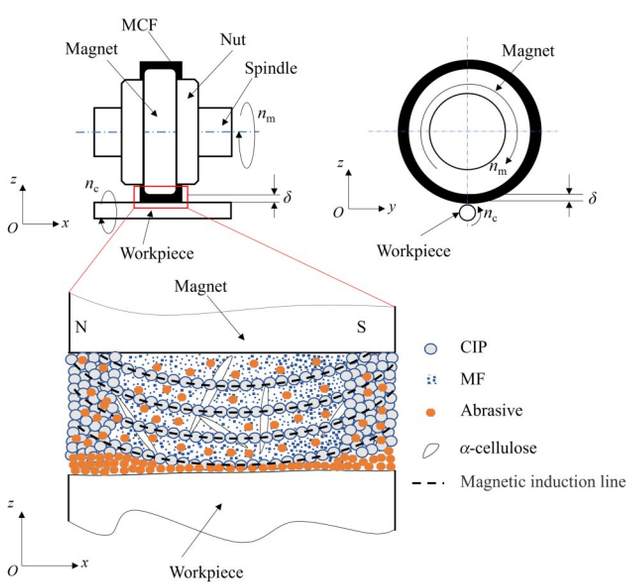

Fig.1 Schematic diagram of MCF polishing wheel

shown in Fig. 2. It can be seen that a ring magnet is mounted on the spindle to form the polishing wheel, which is driven by a servo motor through a synchronous belt. The tube, driven by the motor spindle, is positioned directly below the polishing wheel, which is secured on the clamping device. The working gap δ between the tube and polishing wheel can be manually adjusted using the turntable.

MCF used in this research was composed of CIPs, α-cellulose, abrasive particles (Al_2O_3), and water-based MF containing nanometer-sized Fe_3O_4, as listed in Table 1. The experiment conditions are shown in Table 2. Nd-Fe-B permanent magnet was used as the magnetic field generating device, and the stainless steel tube was chosen as the workpiece. The outer surface of the stainless steel tube was polished under different experiment parameters. In order to ensure the performance of MCF slurry, MCF polishing liquid on the polishing wheel was placed for 25 min for polishing. After polishing, the workpiece was cleaned by an ultrasonic cleaner. Then, the polishing area of the workpiece was measured by a stylus surface roughness meter (SJ-410, Mitutoyo) and a white light interferometer (ZeGagePro, Zygo).

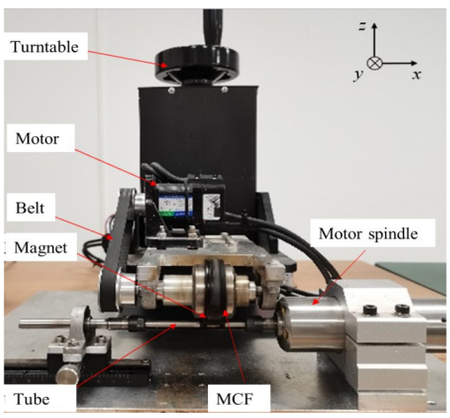

Fig.2 Appearance of MCF polishing device

Table 1 Components of MCF in this research

Component	Concentration/ wt%	Mean diameter
CIP	50	7, 10, 15, and 20 μm
α-cellulose	3	-
Abrasive particle (Al_2O_3)	12	3, 5, 7, and 10 μm
Water-based MF	35	10 nm

4 Results and Discussions

The workpiece surface after polishing for 100 min is shown in Fig. 3. It can be seen that the workpiece surface is matte before polishing, and it is mirror-like after polishing, which indicates that the surface quality is significantly improved. As shown in Fig. 4a, the surface roughness decreases from 0.411 μm to 0.007 μm after polishing, so the workpiece surface roughness reduction rate is 98.297%. The polished workpiece surface is smoother, and the polishing effect is significant. As shown in Fig. 4b, MR depth at both ends of the polishing area is significantly larger than that in the middle area. In the middle of the polishing wheel, MR depth is about 3.5 μm, but it is approximately 12 μm at the end side of the polishing area.

In order to investigate the difference of MR in the polishing process, the magnetic induction intensity at the workpiece surface was simulated and measured, as shown in Fig. 5. It can be seen that the simulated value and the measured values exhibit the same variation trend. The vertical magnetic induction intensity is zero in the middle of the polishing wheel. It gradually increases along the thickness direction and finally reaches the maximum value at the end area. The horizontal magnetic induction intensity is maximum in the middle area of the polishing wheel, and it gradually decreases along the thickness direction. The total magnetic induction intensity rises slowly from the outside of the ring magnet, but it rises sharply near the edge of the magnet and reaches a

Table 2 Experiment parameters

Parameter	Value
Workpiece	304 stainless steel tube with external diameter of 5 mm, inner diameter of 4 mm, and length of 100 mm
Magnet	Nd-Fe-B with external diameter of 48 mm, inner diameter of 25 mm, and thickness of 8 mm; magnetic induction intensity B=0.4 T
Working gap, δ/mm	0.5
Magnet revolution speed, n_m/r·min^{-1}	100, 200, 300, 400
Workpiece speed, n_c/r·min^{-1}	3000, 4000, 5000, 6000
MCF slurry volume, V/mL	1.5, 2.0, 2.5, 3.0
Polishing time, t/min	100

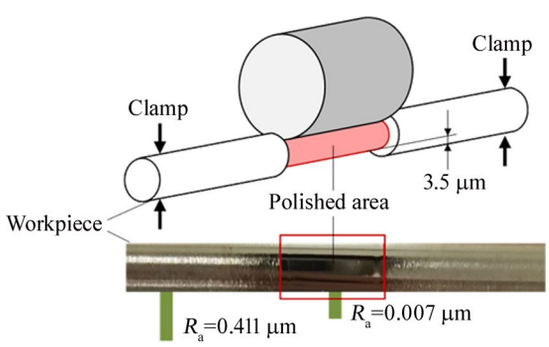

Fig.3 Schematic diagram and appearance of workpiece

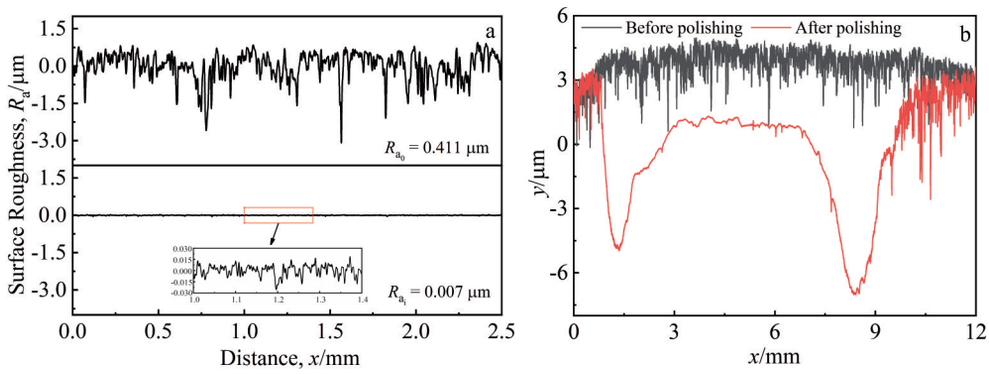

Fig.4 Surface roughness R_a (a) and cross-sectional profile (b) of workpiece before and after polishing

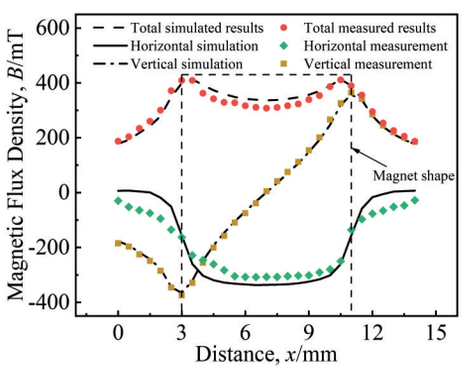

Fig.5 Simulated and measured magnetic induction intensity on workpiece surface

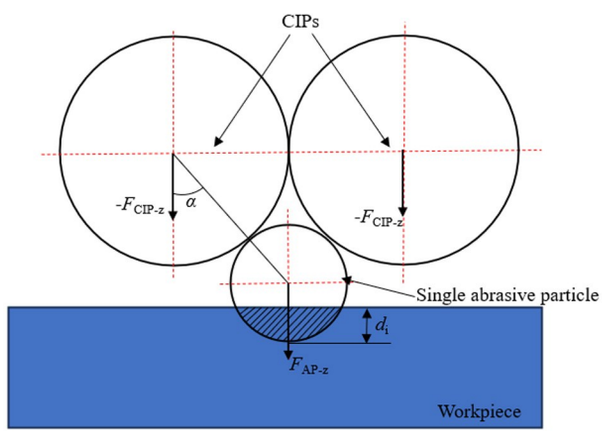

Fig.6 Schematic diagram of force applied by external magnetic field on CIPs and abrasive particle

maximum value at both ends of the magnet (B=0.4 T). During the polishing process, MCF will move to both end sides under the action of extrusion pressure, and an MCF accumulation area will be formed on both end sides of the polishing wheel. It can be found that the magnetic induction intensity is the largest at the end faces of the polishing wheel due to the edge effect of the magnet. Afterwards, MCF accumulates at the edge of the magnet to remove more material, which leads to the nonuniform MR in the polishing area.

4.1 MR model

MR is related to the friction coefficient, polishing pressure, and relative velocity between abrasive particles and workpiece surface in MCF under the action of an external magnetic field. The friction coefficient between abrasive particles and the workpiece surface is constant. MCF polishing pressure on the polishing area changes with the change of magnetic field intensity, resulting in different polishing pressures for particles. The relative speed depends on the magnet speed. To establish a MR model, the force of the magnetic field acting on CIPs and abrasive particles was analyzed, as shown in Fig. 6. When MCF slurry containing abrasive particles is subjected to external magnetic field, magnetic force F_{AP} is applied to abrasive particles. In addition, the magnetic field force F_{CIP} is applied to CIPs located at the top of the abrasive particles. Since CIPs are in equilibrium, an opposite force is applied to the single abrasive particle. Thus, the indentation on the workpiece surface is caused by the magnetic field force generated by the abrasive particles and the opposite magnetic field force in the z direction, denoted as $F_{AP\text{-}z}$ and $F_{CIP\text{-}z}$, respectively. The embedment depth of the abrasive particles on the workpiece surface reflects MR degree during MCF polishing. Therefore, MR can be obtained by Eq. (1), as follows:

$$H_B = \frac{2F_z}{\pi D_{AP}\left(D_{AP} - \sqrt{D_{AP}^2 - D_i^2}\right)} \tag{1}$$

where H_B is the Brinell hardness of the stainless steel workpiece (H_B=180 N/mm^2), F_z is the resultant force of the magnetic field acting on the abrasive particle in z direction, D_{AP} is the abrasive particle diameter, and D_i is the diameter of the indentation formed by the abrasive particle acting on the workpiece surface.

D_i can be expressed by Eq.(2), as follows:

$$D_i = \sqrt{\frac{4F_z}{\pi H_B} - \frac{4F_z^2}{\left(\pi D_{AP} H_B\right)^2}} \tag{2}$$

As shown in Fig.6, F_z can be defined as:

$$F_z = -2F_{CIP\text{-}z}\cos^2\alpha + F_{AP\text{-}z} \tag{3}$$

$$\alpha = \sin^{-1}\frac{D_{CIP}}{D_{CIP} + D_{AP}} \tag{4}$$

where α is angle in Fig.6; D_{CIP} is the diameter of CIP.

The embedment depth of abrasive particles acting on the workpiece surface can be expressed as:

$$d_i = \frac{1}{2}\left(D_{AP} - \sqrt{D_{AP}^2 - D_i^2}\right) \tag{5}$$

where d_i is the embedding depth of a single abrasive particle.

During MCF polishing, CIP in MCF slurry is affected by magnetic force, gravity, viscous resistance, van der Waals force, and buoyancy. Among these forces, the magnetic force is the main factor affecting CIP during polishing. Therefore, the force acting on CIP is:

$$\boldsymbol{F}_{CIP} = \mu_0(\boldsymbol{m}\cdot\nabla)\boldsymbol{H} \tag{6}$$

where μ_0 is the vacuum permeability with $\mu_0=4\pi\times10^{-7}$ N/A^2; $\boldsymbol{m}$ is the magnetic dipole moment of CIP; $\boldsymbol{H}$ is the magnetic field; ∇ represents the Hamiltonian operator. CIP can be regarded as a magnetic dipole due to its extremely small size.

The magnetic dipole moment $\boldsymbol{m}$ is determined by Eq.(7):

$$\boldsymbol{m} = V_{CIP}\chi_m\frac{3\mu_0}{(\mu+2\mu_0)}\boldsymbol{H} \tag{7}$$

where V_{CIP} is the volume of CIP; χ_m is the magnetic susceptibility of CIP with $\chi_m=1\times10^{-3}$; μ is the permeability of CIP with $\mu=5.03\times10^{-7}$ N/A^2.

Define the coordinate system (x, y, z). The Hamiltonian operator ∇ is as follows:

$$\nabla = \frac{\partial}{\partial x}\boldsymbol{i} + \frac{\partial}{\partial y}\boldsymbol{j} + \frac{\partial}{\partial z}\boldsymbol{k} \tag{8}$$

where $\boldsymbol{i}$, $\boldsymbol{j}$, and $\boldsymbol{k}$ are unit vectors in the coordinate system.

Therefore, the magnetic field vector can be obtained through Eq.(9):

$$\boldsymbol{H} = H_x\boldsymbol{i} + H_y\boldsymbol{j} + H_z\boldsymbol{k} \tag{9}$$

where H_x, H_y, and H_z are the components of the magnetic field in the x, y, and z directions, respectively.

The force acting on CIP is expressed as follows:

$$\boldsymbol{F}_{CIP} = F_{CIP\text{-}x}\boldsymbol{i} + F_{CIP\text{-}y}\boldsymbol{j} + F_{CIP\text{-}z}\boldsymbol{k} \tag{10}$$

$$F_{CIP\text{-}z} = \frac{3V_{CIP}\chi_m\mu_0^2}{\mu+2\mu_0}\left(H_x\frac{\partial H_z}{\partial x} + H_y\frac{\partial H_z}{\partial y} + H_z\frac{\partial H_z}{\partial z}\right) \tag{11}$$

where $F_{CIP\text{-}z}$ is the magnetic component acting on CIP in z direction; $\partial H_z/\partial x$, $\partial H_z/\partial y$, and $\partial H_z/\partial z$ are the gradients of H_z in the x, y, and z directions, respectively.

During the polishing process, a single abrasive particle is affected by many forces. Among these forces, the magnetic force is the main factor affecting the abrasive particle, and the force on a single particle is as follows:

$$\boldsymbol{F}_{AP} = -\mu_0 V_{AP}(\boldsymbol{M}\cdot\nabla)\boldsymbol{H} \tag{12}$$

where V_{AP} is the volume of a single abrasive particle; $\boldsymbol{M}$ stands for MF magnetization.

$\boldsymbol{M}$ can also be defined as:

$$\boldsymbol{M} = \chi'_m\boldsymbol{H} \tag{13}$$

where χ'_m is the magnetic susceptibility of MCF with χ'_m= 0.669.

Therefore, the force on a single abrasive particle is:

$$F_{AP} = F_{AP\text{-}x}\boldsymbol{i} + F_{AP\text{-}y}\boldsymbol{j} + F_{AP\text{-}z}\boldsymbol{k} \tag{14}$$

$$F_{AP\text{-}z} = -\mu_0 V_{AP}\chi'_m\left(H_x\frac{\partial H_z}{\partial x} + H_y\frac{\partial H_z}{\partial y} + H_z\frac{\partial H_z}{\partial z}\right) \tag{15}$$

where $F_{AP\text{-}z}$ is the magnetic component acting on abrasive particle in z direction.

Substituting Eq.(11) and Eq.(15) into Eq.(3), the resultant force of a single abrasive particle in z direction can be obtained, as follows:

$$F_z = \left(\frac{6V_{CIP}\chi_m\mu_0^2\cos^2\alpha}{\mu+2\mu_0} + \mu_0 V_{AP}\chi'_m\right) \times\left(H_x\frac{\partial H_z}{\partial x} + H_y\frac{\partial H_z}{\partial y} + H_z\frac{\partial H_z}{\partial z}\right) \tag{16}$$

Since the contact area of MCF polishing wheel and the stainless steel workpiece is approximately a line, the length of the polishing area is equal to the product of the number of active abrasive particles in contact with the workpiece surface and the diameter of abrasive particles.

$$l = N_{AP}D_{AP} \tag{17}$$

where l is the length of the polishing area and N_{AP} is the number of active abrasive particles in contact with the workpiece surface.

The total polishing force of active abrasive particles in the polishing area is:

$$F = N_{AP}F_z \tag{18}$$

Therefore, MR depth d_{MR} is as follows:

$$d_{MR} = \int_0^t d_i N_{AP}\mathrm{d}t \tag{19}$$

Combining Eq.(2), Eq.(5), and Eq.(16–17), d_{MR} is obtained as follows:

$$d_{MR} = \int_0^t \frac{l}{\pi D_{AP}^2 H_B}\left(\frac{6V_{CIP}\chi_m\mu_0^2\cos^2\alpha}{\mu+2\mu_0} + \mu_0 V_{AP}\chi'_m\right) \times\left(H_x\frac{\partial H_z}{\partial x} + H_y\frac{\partial H_z}{\partial y} + H_z\frac{\partial H_z}{\partial z}\right)\mathrm{d}t \tag{20}$$

Substituting each parameter value into Eq. (20), the theoretical MR contour can be obtained, as shown in Fig.7. It can be seen that the variation trend of MR simulation is basically consistent with the experiment value, but there is an error between the fitting curve and the experimental value. This is because the effect of MCF during the experiment is relatively complex, and in addition to the influence of magnetic force on the abrasive particle, the influence of other forces, such as the gravity of the abrasive particle and the

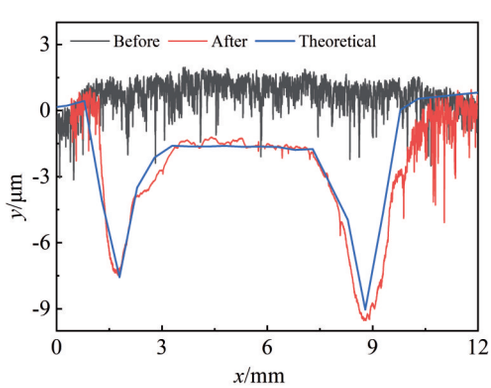

Fig.7 Simulated and experimental MR profiles before and after polishing

buoyancy of the liquid, is not considered.

4.2 Influence of parameters

4.2.1 Influence of CIP particle size

When the polishing conditions are d_{AP}=7 μm, n_m=300 r/min, n_c=4000 r/min, and V=1.5 mL, the influence of iron powder particle size, namely CIP particle size d_{CIP}, on the workpiece surface roughness R_a and reduction rate is shown in Fig. 8. It can be seen that CIP particle size does not affect the reduction of workpiece surface roughness, but the size ratio of iron powder and abrasive particle has an impact on surface quality. When CIP particle size is less than 15 μm, the decreasing trends of surface roughness are the same. When CIP particle size is 15 μm, the surface roughness decrement is large in the first 50 min, and then the surface roughness decrement is small until 100 min. When CIP particle size is 20 μm, the variation trend of reduction rate is similar to that when CIP particle size is 10 μm, but the value is much larger.

Fig. 9 shows the forces on the abrasive particles under different CIP particle sizes, which is obtained according to Fig.6 and Eq.(15). It can be found that when CIP particle size is small, the abrasive particles are subjected to less force, and MR on the workpiece surface is restricted and cannot be effectively removed, resulting in higher surface roughness (R_a= 0.080 μm). With the increase in CIP particle size, the force on the abrasive particles increases, the surface material of the workpiece can be effectively removed, and the surface quality of the workpiece is improved to R_a=0.059 μm. As the CIP particle size continues to increase, it can be found that the force of the wear particle increases rapidly, which causes new scratches on the workpiece surface during MR process, and the final surface roughness is 0.065 μm.

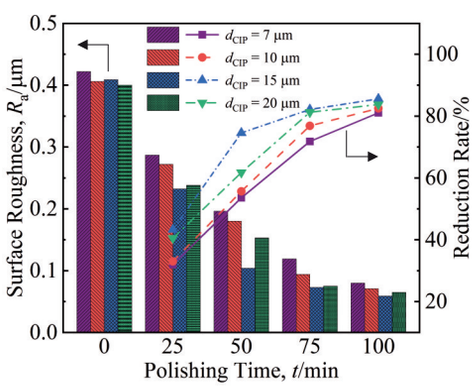

Fig.8 Influence of CIP particle size d_{CIP} on surface roughness R_a and reduction rate

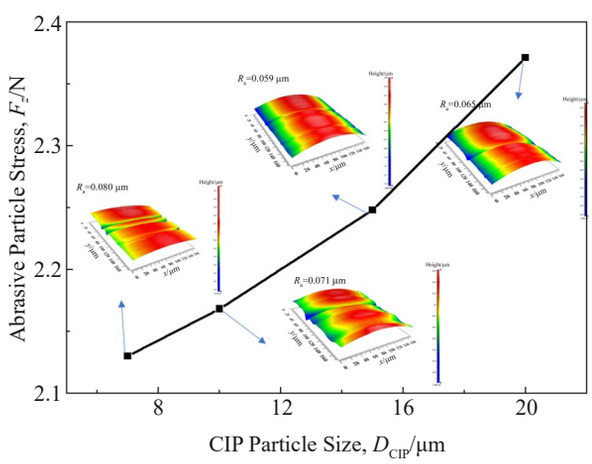

Fig.9 Forces of abrasive particles under different CIP particle sizes

4.2.2 Influence of abrasive particle size

The influence of abrasive particle size d_{AP} on workpiece surface roughness R_a and reduction rate is shown in Fig.10. It can be seen that the surface roughness is decreased with the prolongation of polishing time under all d_{AP} conditions. In the first 75 min of polishing, the surface roughness decreases rapidly, and then the decreasing speed slows down. It is worth noting that when d_{AP}=10 μm, the reduction rate is the largest in the first polishing stage (t≤25 min).

Fig. 11 shows the surface topographies of the workpiece under different abrasive particle sizes. It can be found that the smaller the abrasive particle size, the more the microgullies on the workpiece surface. With the increase in abrasive particle size, the surface pits are gradually reduced. When the abrasive particle size continues to increase, it is found that new defects appear on the workpiece surface. Fig. 12 shows the abrasive particle stress and the number of abrasive particles under different abrasive particle sizes. It can be found that the stress and the number of abrasive particles are inversely proportional. Combined with Fig. 10 and Fig. 11, the surface roughness continues to decrease during polishing within 100 min, but there are still bumps and gullies existing on the surface. At this moment, the surface roughness is 0.085, 0.076, and 0.059 μm when the abrasive particle size is 3, 5, and 7 μm, respectively. A suitable abrasive particle size can promote the removal of surface defects and achieve the optimal surface quality. The continuous increase in abrasive particle size cannot lead to the removal of surface microdefects, and the z-direction force continues to increase, resulting in new scratches on the workpiece surface.

4.2.3 Influence of workpiece rotation speed n_c

Fig. 13 shows the influence of workpiece rotation speed on

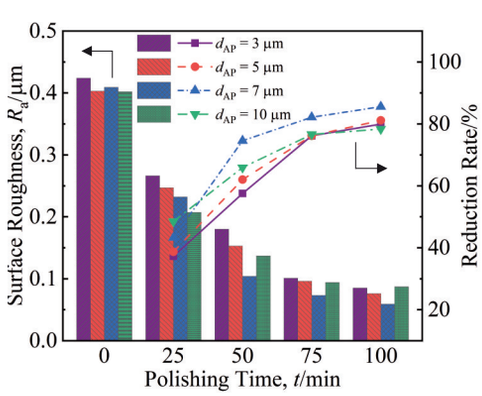

Fig.10 Influence of abrasive particle size d_{AP} on surface roughness R_a and reduction rate

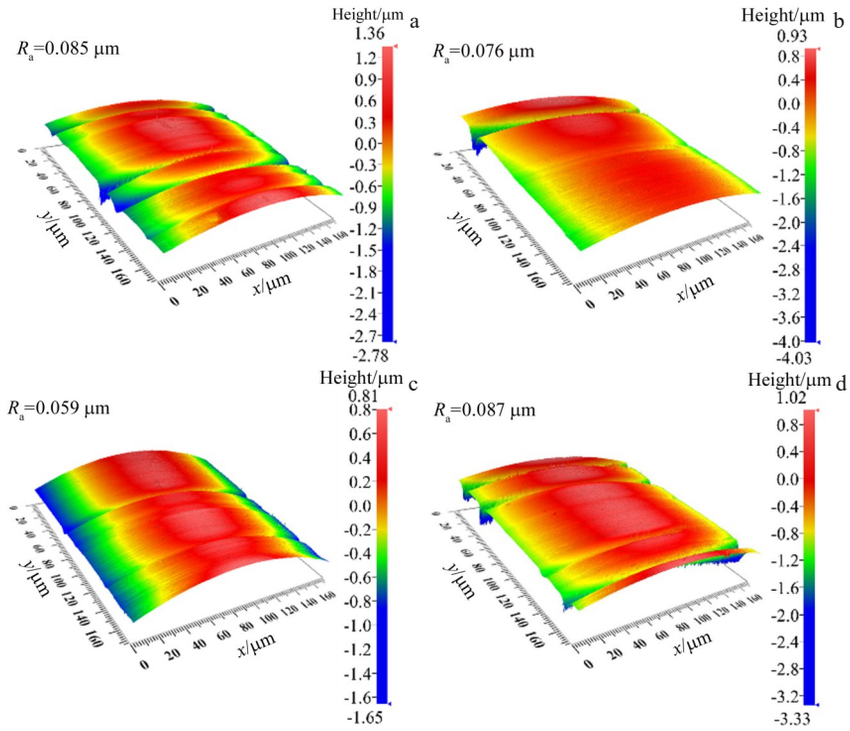

Fig.11 Surface topographies of workpiece under different abrasive particle sizes: (a) 3 μm; (b) 5 μm; (c) 7 μm; (d) 10 μm

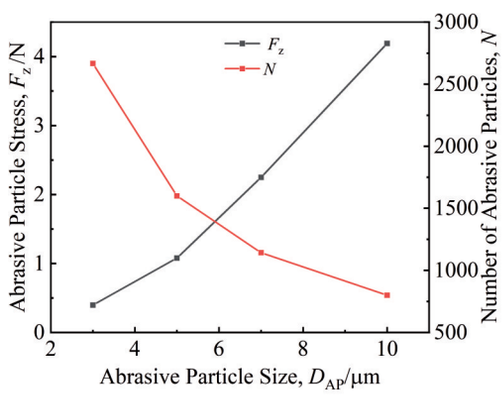

Fig.12 Abrasive particle stress and the number of abrasive particles under different abrasive particle sizes

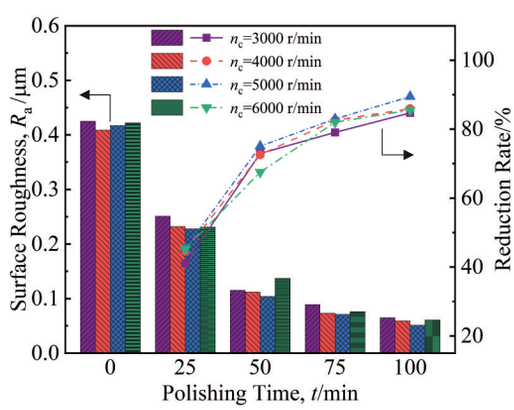

Fig.13 Influence of workpiece rotation speed n_c on surface roughness R_a and reduction rate

surface roughness. It is found that the influence of the workpiece rotation speed on the surface roughness is not very significant: the surface roughness is basically between 50–60 nm, and the variations of reduction rate are basically the same. When the workpiece rotation speed is less than 5000 r/min, because the workpiece rotation speed is low, the abrasive particles will cause scratches on the workpiece surface during the polishing process. When the workpiece rotation speed reaches 5000 r/min, the increase in workpiece rotation speed enhances the polishing effect of the abrasive particles. Therefore, after a long time of polishing, the quality of workpiece surface reaches the best with surface roughness of 0.051 μm, and the surface roughness reduction rate is also the highest of 89.448%. When the workpiece rotation speed is less than 5000 r/min, the quality of workpiece surface deteriorates due to the increase in relative speed, which shortens the contact time of abrasive particles and the workpiece surface, and the surface material cannot be removed in time. According to the Princeton equation:

$$\mathrm{MRR} = kpv \tag{21}$$

where k is the coefficient; p is the pressure of MCF polishing liquid acting on the workpiece; v is the relative speed of motion between the abrasive particle and the workpiece. Thus, the higher the magnet speed within a reasonable range, the faster the MR rate.

Fig. 14 shows the surface topographies of the workpiece at different workpiece rotation speeds. It can be found that there are different degrees of microgullies on the workpiece surface under different workpiece rotation speeds. This is because when the workpiece rotation speed is less than 5000 r/min, the

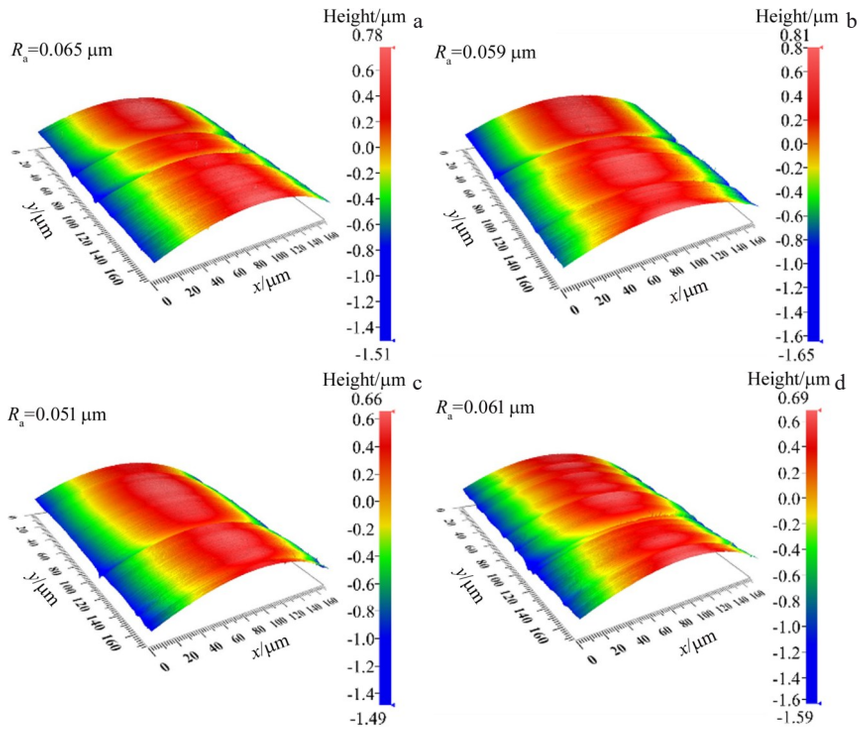

Fig.14 Surface topographies of workpiece at different workpiece rotation speeds: (a) 3000 r/min; (b) 4000 r/min; (c) 5000 r/min; (d) 6000 r/min

relative motion speed between the abrasive particles and the workpiece is slow, and the abrasive particles cannot be effectively updated, resulting in scratches on the workpiece surface caused by the abrasive particles in the polishing process. When the workpiece rotation speed reaches 5000 r/min, the polishing effect of the abrasive particles is enhanced. When the workpiece rotation speed is larger than 5000 r/min, the workpiece surface quality deteriorates due to the increase in relative speed, which shortens the contact time of abrasive particles and the workpiece surface, and the surface material cannot be removed in time.

4.2.4 Influence of magnet speed n_m

In the process of MCF polishing, the speed of abrasive particles directly affects MR on the workpiece surface. Fig. 15 shows the influence of magnet speed n_m on surface roughness and reduction rate. It can be found that regardless of the magnet speed, the workpiece surface roughness decreases. When n_m=200 r/min, the surface roughness gradually decreases, reaching the best surface roughness of 0.042 μm, and the reduction rate reaches the maximum value of 90.749%. When n_m=100 r/min, it is found that the decreasing trend of surface roughness is basically the same as that when n_m=200 r/min, but the polishing effect is far less significant than that when n_m=200 r/min, which indicates that when the relative motion between the abrasive particles and the workpiece surface is slow, MR amount on the workpiece surface is small. When the magnet speed is 300 r/min, the reduction rate in the first 25 min is higher than that when the magnet speed is 200 r/min, which is because the relative speed between the abrasive particles and the workpiece surface is also fast at higher magnet speeds, and the workpiece surface material can be effectively removed. In the subsequent polishing process, the polishing efficiency at n_m=300 r/min is lower than that at n_m=200 r/min.

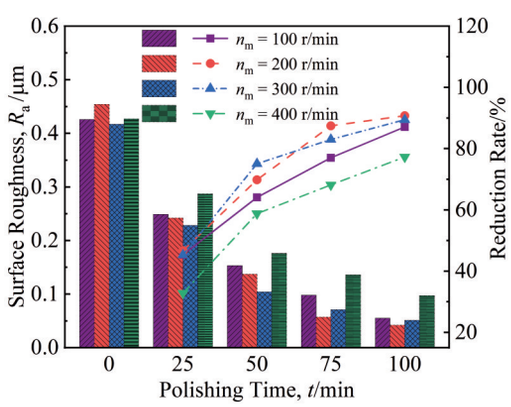

Fig.15 Influence of magnet speed n_m on surface roughness R_a and reduction rate

Fig. 16 shows the surface topographies of the workpiece at different magnet speeds. It can be seen that the increase in magnet speed does not promote MR. When the magnet speed is 400 r/min, the workpiece surface roughness reaches 0.097 μm, and MR effect on the workpiece surface is inferior. This is because the centrifugal force of the abrasive particles is greater than the magnetic field force. Thus, the abrasive particles begin to detach from the magnetic cluster, and the reduction in the number of abrasive particles leads to a decrease in polishing efficiency. As the magnet speed continues to increase, the surface quality becomes worse, indicating that not only will the abrasive particles be detached, but

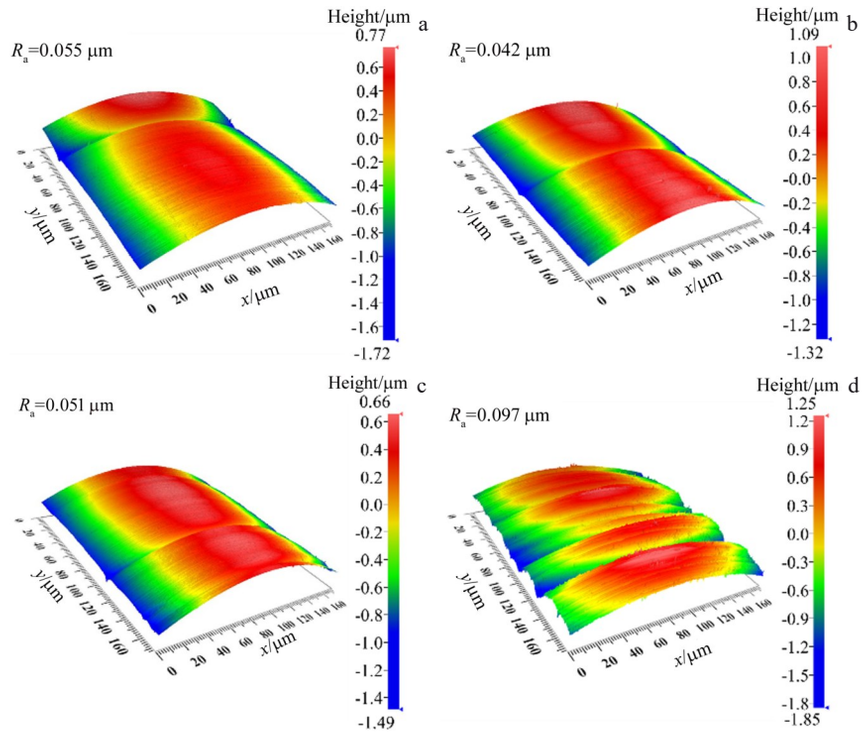

Fig.16 Surface topographies of workpiece at different magnet speeds: (a) 100 r/min; (b) 200 r/min; (c) 300 r/min; (d) 400 r/min

also the abrasive chain failure or dislocation occurs, resulting in a small amount of MR and inferior surface roughness.

4.2.5 Influence of supply amount V

The influence of supply amount V on workpiece surface roughness and reduction rate is shown in Fig. 17. It can be seen that regardless of the supply amount, the workpiece surface roughness decreases during the polishing process. When the supply amount is 2.0 mL, the reduction rate is 90.749%. With the increase in supply amount, the reduction rate is gradually accelerated. When the supply amount is 2.0 mL, the reduction rate is the highest of 98.297%, and the surface roughness also reaches the lowest of 0.007 μm. As the supply amount continues to increase, it can be found that the increase in supply amount does not affect the surface roughness.

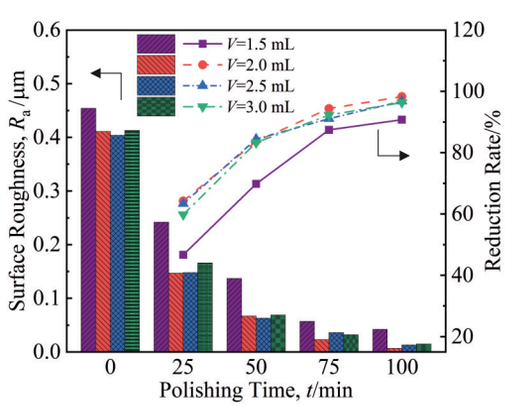

Fig.17 Influence of supply amount V on surface roughness R_a and reduction rate

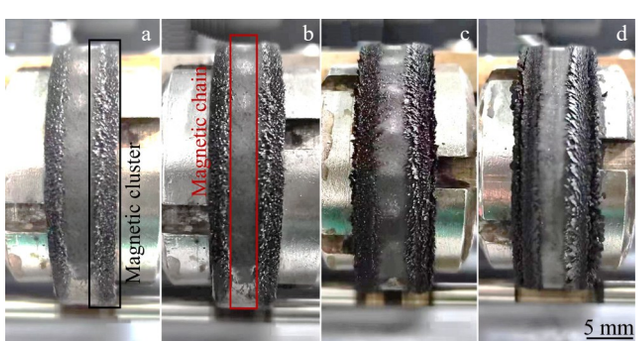

Fig.18 MCF appearances under different supply amounts: (a) 1.5 mL; (b) 2.0 mL; (c) 2.5 mL; (d) 3.0 mL

Fig. 18 shows the MCF appearances under different supply amounts. It can be found that MCF forms a short cluster structure at the edge of the magnet, and the middle part of the magnet forms a closed magnetic chain. The formation of the MCF structure is determined by the magnetic field distribution, and this structural combination is the main reason for the large MR on both sides of the workpiece surface profile and the small MR in the middle area. Under low supply amount, MCF is not fully formed, and the reduction rate of workpiece surface roughness is small. With the increase in supply amount, MCF has two structures to achieve precision machining of the workpiece. With the further increase in supply amount, magnetic clusters also begin to appear in the closed area of the magnetic field line, leading to scratches on the workpiece surface, which is not conducive to improve the surface quality of the workpiece.

Fig. 19 shows the surface topographies of the workpiece

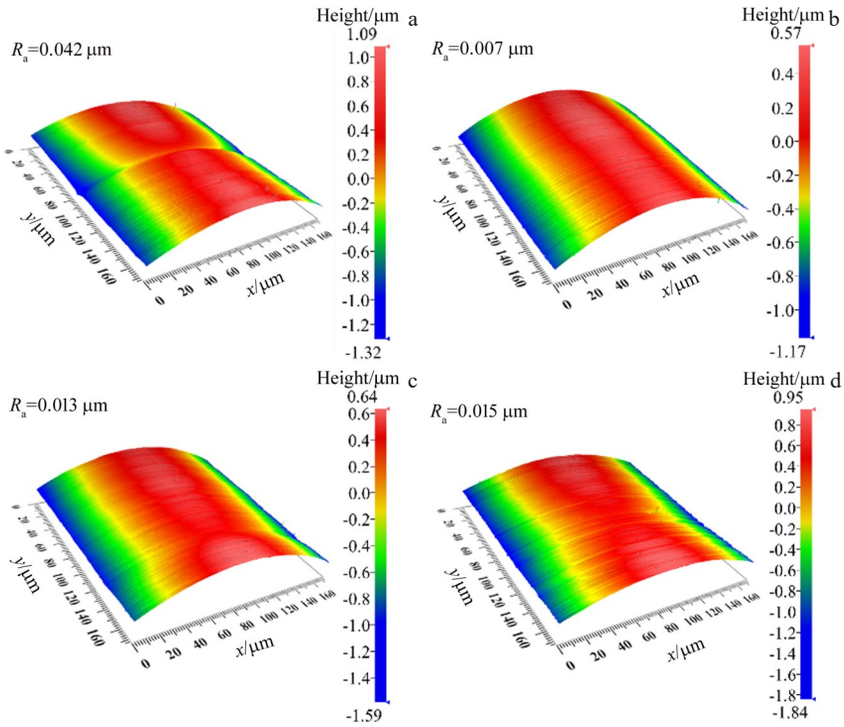

Fig.19 Surface topographies of workpiece under different supply amounts: (a) 1.5 mL; (b) 2.0 mL; (c) 2.5 mL; (d) 3.0 mL

under different supply amounts. It can be found that there are still defects on the workpiece surface when V=1.5 mL, and there are no defects on the workpiece surface when V=2.0 mL. The pits and microgullies on the workpiece surface are completely removed, and the surface quality of the workpiece is optimal. The workpiece surface under V=2.5 mL condition is smooth. There are no obvious pits or gullies, resulting in the reduction of roughness. The workpiece surface under V=3.0 mL condition also has no obvious defects, but there are still small gullies. This is because too much supply leads to excessive abrasive particles acting on the workpiece surface, causing new scratches on the workpiece surface. Appropriate supply can make MCF polishing liquid contain enough abrasive particles in the polishing process to contact with the workpiece surface, so as to achieve the efficient removal of material on the workpiece surface. During the polishing process, partial MCF will be extruded and piled up on one end of the polishing wheel due to the working gap and magnetic induction intensity, resulting in inconsistent MCF at both ends of the MCF polishing wheel and leading to rough polishing area. Besides, excessive MCF provides excessive abrasive particles. Some new scratches will inevitably appear in the polishing process.

Briefly, using the polishing wheel processing method of MCF, MCF forms a Bingham fluid with higher viscosity under the action of an external magnetic field, and less MCF can be used to achieve efficient precision machining of stainless steel tubes. The optimal MCF components should be 50wt% CIPs (CIP size d_{CIP}=15 μm), 12wt% abrasive particles (abrasive particle size d_{AP}=7 μm), 3wt% α-cellulose, and 35wt% MF with processing gap δ of 0.5 mm. The optimal processing parameters of MCF polishing wheel are magnet speed n_m=200 r/min, workpiece speed n_c=5000 r/min, and supply amount V=2.0 mL.

5 Conclusions

1) Using the polishing wheel processing method of MCF, MCF forms a Bingham fluid with higher viscosity under the action of an external magnetic field, and less MCF can be used to achieve efficient precision machining of stainless steel tubes.

2) The established MR model has high accuracy. The error is because only the effect of magnetic force on abrasive particles and iron powder particles is considered. Other effects are ignored.

3) The optimal MCF components should be 50wt% CIPs (CIP size d_{CIP}=15 μm), 12wt% abrasive particles (abrasive particle size d_{AP}=7 μm), 3wt% α-cellulose, and 35wt% MF with processing gap δ of 0.5 mm. The optimal processing parameters of MCF polishing wheel are magnet speed n_m=200 r/min, workpiece speed n_c=5000 r/min, and supply amount V=2.0 mL.

References

1 Zou Zichuan, He Lin, Zhou Tao *et al*. *Journal of Manufacturing Processes*[J], 2022, 83: 535

2 Xavior M, Adithan M. *Mater Process Technology*[J], 2009, 209(2): 900

3 Chen Jiajun, Song Xiping, Wang Han *et al*. *Rare Metal Materials and Engineering*[J], 2018, 47(9): 2642 (in Chinese)

4 Raval A, Choubey A, Engineer C *et al*. *Materials Science and Engineering A*[J], 2004, 386: 33

5 Ji Shiwei, Huang Nan, Wan Guojiang *et al*. *Journal of Clinical Rehabilitative Tissue Engineering Research*[J], 2011, 16(15): 2851

6 Tyulagin P E, Mishina E S, Polyakova A S *et al*. *Russian Journal of Inorganic Chemistry*[J], 2023, 68(5): 610

7 Chen Jiapeng, Peng Yanan, Wang Zhankui *et al*. *International Journal of Advanced Manufacturing Technology*[J], 2024, 131(5–6): 2667

8 Ni Cong, Shi Yan. *Materials and Manufacturing Processes*[J], 2023, 38(5): 529

9 Choudhary Shubham, Duvedi Ravinder Kumar, Saini Jaswinder Singh. *Proceedings of the Institution of Mechanical Engineers Part E-Journal of Process Mechanical Engineering*[J], 2024, 238(1): 383

10 Khatekar Nikhil, Pawade Raju. *International Journal of Advanced Manufacturing Technology*[J], 2019, 104(5–8): 3083

11 Loh Yeeman, Cheung Chifai, Wang Chunjin *et al*. *Micromachines*[J], 2022, 13(7): 1060

12 Yuan Julong, Zhang Feihu, Dai Yifa *et al*. *Journal of Mechanical Engineering*[J], 2010, 46(15): 161

13 Yin Shaohui, Xu Zhiqiang, Duan Hongjie *et al*. *Advanced Materials Research*[J], 2013, 797: 396

14 Odenbach S. *Journal of Physics: Condensed Matter*[J], 2004, 16(32): R1135

15 Alberto N, Domingues M F, Marques C *et al*. *Sensors*[J], 2018, 18(12): 4325

16 Yu J, Chen D, Cai Z *et al*. *Journal of Magnetism and Magnetic Materials*[J], 2019, 492: 165678

17 Ashtiani M, Hashemabadi S H, Ghaffari A. *Journal of Magnetism and Magnetic Materials*[J], 2015, 374: 716

18 Bai Y, Zhang X, Yang C *et al*. *Light: Advanced Manufacturing*[J], 2022, 3(4): 630

19 Bahl S, Nagar H, Singh I *et al*. *Materials Today: Proceedings*[J], 2020, 28: 1302

20 Shimada K, Akagami Y, Kamiyama S *et al*. *Journal of Intelligent Material Systems and Structures*[J], 2002, 13(7–8): 405

21 Wang Y, Wu Y, Guo H *et al*. *Journal of Applied Physics*[J], 2014, 117(17): 298

22 Shimada K, Fujita T, Oka H *et al*. *Transactions of the Japan Society of Mechanical Engineers*[J], 2001, 67: 3034

23 Guo Huiru, Wu Yongbo, Li Yaguo *et al*. *Key Engineering Materials*[J], 2012, 523–524: 161

24 Guo Huiru, Wu Yongbo, Lu Dong *et al*. *Journal of Materials Processing Technology*[J], 2014, 214(11): 2759

25 Wang Youliang, Wu Yongbo, Nomura M *et al*. *Precision Engineering*[J], 2016, 45: 67

26 Wang Youliang, Wu Yongbo, Nomura M *et al*. *Precision Engineering*[J], 2017, 48: 32

27 Wang Youliang, Liang Bo, Zhang Wenjuan. *Rare Metal Materials and Engineering*[J], 2024, 53(2): 377

28 Fan J, Ren X, Pan R *et al*. *International Journal of Advanced Manufacturing Technology*[J], 2022, 121(3–4): 2181

29 Jiao Li, Wu Yongbo, Guo Huiru. *Journal of Mechanical Engineering*[J], 2013, 49(17): 79

30 Feng M, Wu Y, Wang Y Z *et al*. *Precision Engineering*[J], 2020, 65: 216

利用磁性复合流体轮对管材外表面进行超精密抛光

王有良[1,2]，姜　哲[1]，张文娟[3]，尹新城[1,2]，梁　博[1]

(1. 兰州理工大学 机电工程学院，甘肃 兰州 730050)

(2. 兰州理工大学 数字制造技术与应用教育部重点实验室，甘肃 兰州 730050)

(3. 兰州理工大学 省部共建有色金属先进加工与再利用国家重点实验室，甘肃 兰州 730050)

摘　要：提出了一种采用磁性复合流体（MCF）轮对不锈钢管外表面进行抛光的新方法。首先，构建了抛光装置，并通过Maxwell软件和特斯拉计探讨了MCF轮在工件表面的磁场分布，研究了磁场分布与工件表面材料去除（MR）之间的关系。然后，建立了MR模型，并通过给定条件下的实验结果验证了该模型。最后，通过实验研究了羰基铁粉粒径d_{CIP}、磨料粒径d_{AP}、磁铁转速n_m、工件转速n_c以及MCF供给量V对表面粗糙度R_a和减少率的影响规律，并探讨了不同参数对表面质量的作用机制。结果表明，抛光过程中的磁感应强度与工件的抛光轮廓呈正相关。MR仿真的趋势与实验值一致，证明了MR模型的准确性。在磁铁转速n_m=200 r/min和工件转速n_c=5000 r/min条件下，使用含有50wt%羰基铁粉（15 μm）、12wt%磨料颗粒（7 μm）、3wt% α-纤维和35wt%磁性液体的MCF浆料（V=2 mL），不锈钢管的表面粗糙度从0.411 μm降低到0.007 μm，抛光100分钟后，表面粗糙度的减少率达98.297%，证明了这种方法适用于管材外表面的抛光。

关键词：磁性复合流体；不锈钢管；抛光；表面粗糙度

作者简介：王有良，男，1986年生，博士，副教授，兰州理工大学机电工程学院，甘肃 兰州 730050，E-mail：wangyouliang20@163.com